

—●— Technology Review —●—

Rapid Structure-Activity and Selectivity Analysis of Kinase Inhibitors by BioMAP Analysis in Complex Human Primary Cell-Based Models

Eric J. Kunkel,¹ Ivan Plavec,¹ Dat Nguyen,¹ Jennifer Melrose,¹ Elen S. Rosler,¹ Leon T. Kao,¹ Yuker Wang,¹ Evangelos Hytopoulos,¹ Anthony C. Bishop,² Raynard Bateman,² Kevan M. Shokat,² Eugene C. Butcher,^{3,*} and Ellen L. Berg^{1,*}

Abstract: Rapid, quantitative methods for characterizing the biological activities of kinase inhibitors in complex human cell systems could allow the biological consequences of differential target selectivity to be monitored early in development, improving the selection of drug candidates. We have previously shown that Biologically Multiplexed Activity Profiling (BioMAP) permits rapid characterization of drug function based on statistical analysis of protein expression data sets from complex primary human cell-based models of disease biology. Here, using four such model systems containing primary human endothelial cells and peripheral blood mononuclear cells in which multiple signaling pathways relevant to inflammation and immune responses are simultaneously activated, we demonstrate that BioMAP analysis can detect and distinguish a wide range of inhibitors directed against different kinase targets. Using a panel of p38 mitogen-activated protein kinase antagonists as a test set, we show further that related compounds can be distinguished by unique features of the biological responses they induce in complex systems, and can be classified according to their induction of shared (on-target) and secondary activities. Statistical comparisons of quantitative BioMAP profiles and analysis of profile features allow correlation of induced biological effects with chemical structure and mapping of biological responses to chemical series or substituents on a common scaffold. Integration of automated BioMAP analysis for prioritization of hits and for structure-activity relationship studies may improve and accelerate the design and selection of optimal therapeutic candidates.

Introduction

PROTEIN KINASES ARE ATTRACTIVE DRUG TARGETS for a number of disease indications.¹ Protein phosphorylation by kinases plays a central role in the control and

regulation of signaling pathways in all cells, suggesting that selective targeting of key kinases that regulate disease-specific mechanisms may offer safe and effective therapies. However, the development of protein kinase inhibitors remains challenging because most inhibitors

¹BioSeek, Inc., Burlingame, CA.

²Department of Cellular and Molecular Pharmacology, University of California, San Francisco, CA.

³Laboratory of Immunology and Vascular Biology, Department of Pathology, Stanford University School of Medicine, Stanford, CA.

*These authors are co-senior authors.

ABBREVIATIONS: BioMAP, Biologically Multiplexed Activity Profiling; CaMKII, Ca²⁺/calmodulin-dependent protein kinase II; Cdk, cyclin-dependent kinase; CK2, casein kinase 2; DAF, decay accelerating factor; DRB, 5,6-dichloro-1- β -D-ribofuranosylbenzimidazole; ELISA, enzyme-linked immunosorbent assay; FDR, false detection rate; GSK-3 β , glycogen synthase kinase 3 β ; HMG-CoA, 3-hydroxy-3-methyl-glutaryl coenzyme A; Hsp90, heat shock protein 90; HUVEC, human umbilical vein endothelial cells; ICAM-1, intercellular adhesion molecule-1; IFN- γ , interferon- γ ; IL, interleukin; IMPDH, inosine 5'-monophosphate dehydrogenase; JAK, Janus kinase; LPS, lipopolysaccharide; MAPK, mitogen-activated protein kinase; MEK, mitogen-activated protein kinase kinase; NF- κ B, nuclear factor- κ B; PBMC, peripheral blood mononuclear cells; PI-3K, phosphatidylinositol 3-kinase; PKA, protein kinase A; PPAR, peroxisome proliferation-activated receptor; PTK, protein tyrosine kinase; SAG, superantigen; SAR, structure-activity relationship; siRNA, small interfering RNA; TBB, 4,5,6,7-tetrabromo-2-aza-benzimidazole; TNF- α , tumor necrosis factor- α ; uPAR, urokinase-type plasminogen activator receptor; VCAM, vascular cell adhesion molecule; VEGFR, vascular endothelial growth factor receptor.

interact with the ATP-binding pocket and thus have the potential to inhibit multiple targets. Canvassing large numbers of kinases for cross-reactivity in biochemical assays can be helpful in identifying selectivity problems, but is limited by the number of kinase assays available and the fact that there are ≥ 500 human protein kinase genes.² In addition, for all chemical entities, and not just inhibitors of protein kinases, there is the chance of interactions with unexpected secondary targets involving compound features outside the target interface.

We have recently described an approach (Biologically Multiplexed Activity Profiling, or BioMAP profiling) for the characterization of drug function using complex, primary human cell-based models of disease biology.³ In these models, biological complexity is provided by (a) the activation of multiple signaling pathways, (b) interactions of multiple primary human cell types, and (c) the use of multiple biological systems for data analysis. By providing conditions where multiple pathways are active, cell types are allowed to interact, and activities are assessed in multiple "systems" (cell plus environment combinations) relevant to inflammation and immune biology, compounds from many different mechanistic classes can be detected and distinguished. These include inhibitors of cytokines [*e.g.*, tumor necrosis factor- α (TNF- α) antagonists], kinase and enzyme inhibitors [*e.g.*, p38 mitogen-activated protein kinase (MAPK), MAPK kinase-1/2 (MEK1/2), phosphatidylinositol 3-kinase (PI-3K), 3-hydroxy-3-methyl-glutaryl coenzyme A (HMG-CoA) reductase, inosine 5'-monophosphate dehydrogenase (IMPDH)], inhibitors of signaling adaptors [*e.g.*, calcineurin, heat shock protein 90 (Hsp90)], as well as modulators of nuclear receptors [*e.g.*, glucocorticoids, peroxisome proliferator-activated receptor (PPAR) agonists]. BioMAP profiling is automated and scalable, and results are quantitative and reproducible and provide insight into biological activities in a rapid and practical manner without requiring large numbers of molecular measurements. BioMAP profiling has already been used to (a) correlate functional responses of drugs to mechanism class, (b) identify secondary target activities, (c) provide insights into and generate hypotheses regarding mechanisms that underlie clinical activities of approved therapeutics, and (d) characterize gene function networks.^{3,4}

The broad sensitivity of BioMAP assays for compounds from many different mechanistic classes suggests application of this technology to structure-activity relationship (SAR) studies, as the breadth of pathways and mechanisms affecting BioMAP profiles should allow ready identification and classification of off-target or secondary activities. SAR in BioMAP assays can potentially allow optimization, or at least monitoring, of multiple aspects of the biological activity of lead analogues during the optimization process. The present study demonstrates the use of BioMAP profiling to define SARs within a se-

ries of trisubstituted imidazole inhibitors of p38 MAPK. Modifications at both ends of the core structure regulate the appearance of secondary activities, illustrating the value of integrating complex biological systems analysis for fine-tuning compound selection. Profiling in BioMAP systems can be used throughout the drug development process by identifying secondary activities and discriminating core functional activities for selection of lead candidates (this article) and by revealing biological responses and secondary activities that can contribute to both positive and negative side effects in animal studies and in patients.³

Materials and Methods

Cytokines, antibodies, and reagents

Recombinant human interferon- γ (IFN- γ), TNF- α , interleukin (IL)-1 β , and IL-4 were from R&D Systems (Minneapolis, MN). Histamine was from Sigma (St. Louis, MO). Mouse antibodies were obtained from commercial sources: murine IgG and anti-human vascular endothelial growth factor receptor-2 (VEGFR2) (mIgG1; Sigma), anti-human tissue factor (mIgG1; Calbiochem, San Diego, CA), anti-human intercellular adhesion molecule-1 (ICAM-1) (mIgG1; Beckman Coulter, Fullerton, CA), and anti-human E-selectin (mIgG1; HyCult Biotechnology, Uden, The Netherlands). Mouse antibodies against human vascular cell adhesion molecule-1 (VCAM-1) (mIgG1), HLA-DR (mIgG2a), CD3 (mIgG1), CD40 (mIgG1), CD69 (mIgG1), MIG (mIgG1), MCP-1 (mIgG1), CD14 (mIgG1), IL-1 α (mIgG1), P-selectin (mIgG1), DAF (mIgG2a), urokinase-type plasminogen activator receptor (uPAR) (mIgG1), and CD38 (mIgG1) were obtained from BD Biosciences (San Jose, CA). Mouse antibodies against eotaxin-3 (mIgG1), IL-8 (mIgG1), and M-CSF (mIgG1) were obtained from R&D Systems. Apigenin, wortmannin, GW8510, GW5074, UO126, and genistein were obtained from Sigma. PD098059, H-89, glycogen synthase kinase 3 β (GSK-3 β) inhibitor II, SB202190, SB203580, 4,5,6,7-tetra-bromo-2-aza-benzimidazole (TBB), BAY43-9006, H-1152, PD169316, SKF-86002, WHI-P131, ZM39923, AG490, AG126, SB239063, and SB220025 were from Calbiochem. 5,6-dichloro-1- β -D-ribofuranosylbenzimidazole (DRB), PP2, and PP1 were from BIOMOL (Plymouth Meeting, PA). ZM336372, KN-62, SB415286, SB216763, kenpaullone, roscovitine, SP600125, and LY294002 were from Tocris (Ellisville, MO). Staphylococcal enterotoxin B, toxic shock syndrome toxin-1 (staphylococcal enterotoxin F) from *S. aureus* (collectively called superantigen; SAG), and lipopolysaccharide (LPS) from *Salmonella enteritidis* were obtained from Sigma. SB203580 analogues were synthesized and purified by flash chromatography, and structures were verified by ¹H

NMR and mass spectroscopy as described.⁵ IC₅₀ values for inhibition of p38 α for each compound were determined as described.⁵

Cell culture

Human umbilical vein endothelial cells (HUVEC) were cultured as described.³ Peripheral blood mononuclear cells (PBMC) were prepared from buffy coats (Stanford Blood Bank, Stanford, CA) by centrifugation over Hisopaque-1077 (Sigma). Four assay systems, 3C, 4H, SAG, and LPS, were used. For the 3C system, HUVEC were cultured for 24 h in microtiter plates (Falcon; BD Biosciences), in the presence of cytokines IL-1 β (1 ng/ml), TNF- α (5 ng/ml), and IFN- γ (20 ng/ml). For the 4H system, HUVEC were cultured in the presence of IL-4 (5 ng/ml) and histamine (10 μ M). For the SAG system, HUVEC were cultured with PBMC (7.5×10^4) and SAG (20 ng/ml). For the LPS system, HUVEC were cultured with PBMC (7.5×10^4) and LPS (2 ng/ml). Compounds were added 1 h before stimulation and were present during the entire 24-h stimulation period. Cell-based enzyme-linked immunosorbent assay (ELISAs) were carried out as described.³

Small interfering RNA (siRNA) transfection

HUVEC cells were resuspended at 2×10^6 cells in 100 μ l of Nucleofection solution (Human Umbilical Vein Endothelial Cell Nucleofactor Kit, AMAXA, Koeln, Germany). An siRNA targeting both MEK3 and MEK6 (GTGGCTACTTGGTGGACTC; 15 μ l of a 20 μ M solution; Dharmacon, Lafayette, CO) or a scrambled control siRNA was added to the cell suspension, transferred into an electroporation cuvette, and electroporated using the U-1 setting. The cell suspension was then transferred into a separate tube containing 3 ml of EGM-2 media (Clonetics), incubated at 37°C for 10 min, and plated into microtiter plates (25,000 cells/well) for cytokine activation and ELISA analysis as described above. Effective ($\geq 80\%$) reduction of target mRNA levels in siRNA-transfected cells was confirmed by quantitative RT-PCR.

Data analysis

Mean optical density values for each parameter measured by ELISA were calculated from triplicate samples per experiment. Well-to-well coefficients of variance range from 1 to 12%, depending on the parameter measured, and average 5% across all controls. Day-to-day variability for a given readout, system, and treatment is the greatest contributor to the overall variability (ranging from 10 to 60% of the total variability), but is controlled for by using a prediction envelope to give the error boundaries for all the measurements simultaneously, consistent with our multivariate analysis approach. The en-

velope estimates the variability of the measurements around the mean (all data are centered). By combining similar measurements from multiple experiments, we establish overall error measures for our experiments while eliminating the specific bias of each experiment. We have performed extensive studies concerning the number of repeats required for correctly classifying repeated profiles within given confidence limits leading to the requirement for at least three replicate wells per treatment and at least three independent repeats (unpublished observations). Within each experiment, mean optical density values were used to generate ratios between treated (*e.g.*, compound or siRNA) and matched control (*e.g.*, media or dimethyl sulfoxide) parameter values. These normalized parameter ratios were then log₁₀ transformed. For profile plots, the means \pm SEM from three or more experiments are shown. Log expression ratios were used in all Pearson correlation calculations. For heat maps, averaged profile data were ordered in the correlation plot by coupling multidimensional scaling and pivoting to move high correlations toward the diagonal. For Function Similarity Maps, correlations were visualized in two dimensions by multidimensional scaling using AT&T GraphViz software. Distances between compounds are representative of their similarities, and lines are drawn between compounds whose profiles are similar at a level not due to chance. Significant correlations were determined by (a) identifying the number of correlations that exceed a given threshold in the observed Pearson correlation distribution of the profiles, (b) calculating the average number of Pearson correlations that exceed this threshold using correlations calculated from randomized data made by permuting the empirical profiles multiple times, (c) reselecting the Pearson correlation threshold to minimize the false detection rate (FDR) (the FDR provides the probability that a significant correlation is a false positive), and (d) applying this cutoff Pearson correlation value to the correlations between experimental profiles. This ensures that for a 5% FDR, 95% of the correlations derived from the experimental profiles are not due to chance.

Results

Mechanistic discrimination of kinase inhibitors by BioMAP analysis in complex primary human cell-based assays

We have previously shown that a wide range of biologically active agents and drugs can be detected and distinguished by BioMAP profiling in primary human cell-based model systems comprising endothelial cells and/or PBMC in co-culture with specific activating stimuli.^{3,4} Figure 1A lists targets and pathways shown to be detected and distinguished by BioMAP profiling in the four BioMAP assay “systems” (3C, 4H, LPS, and SAG) shown

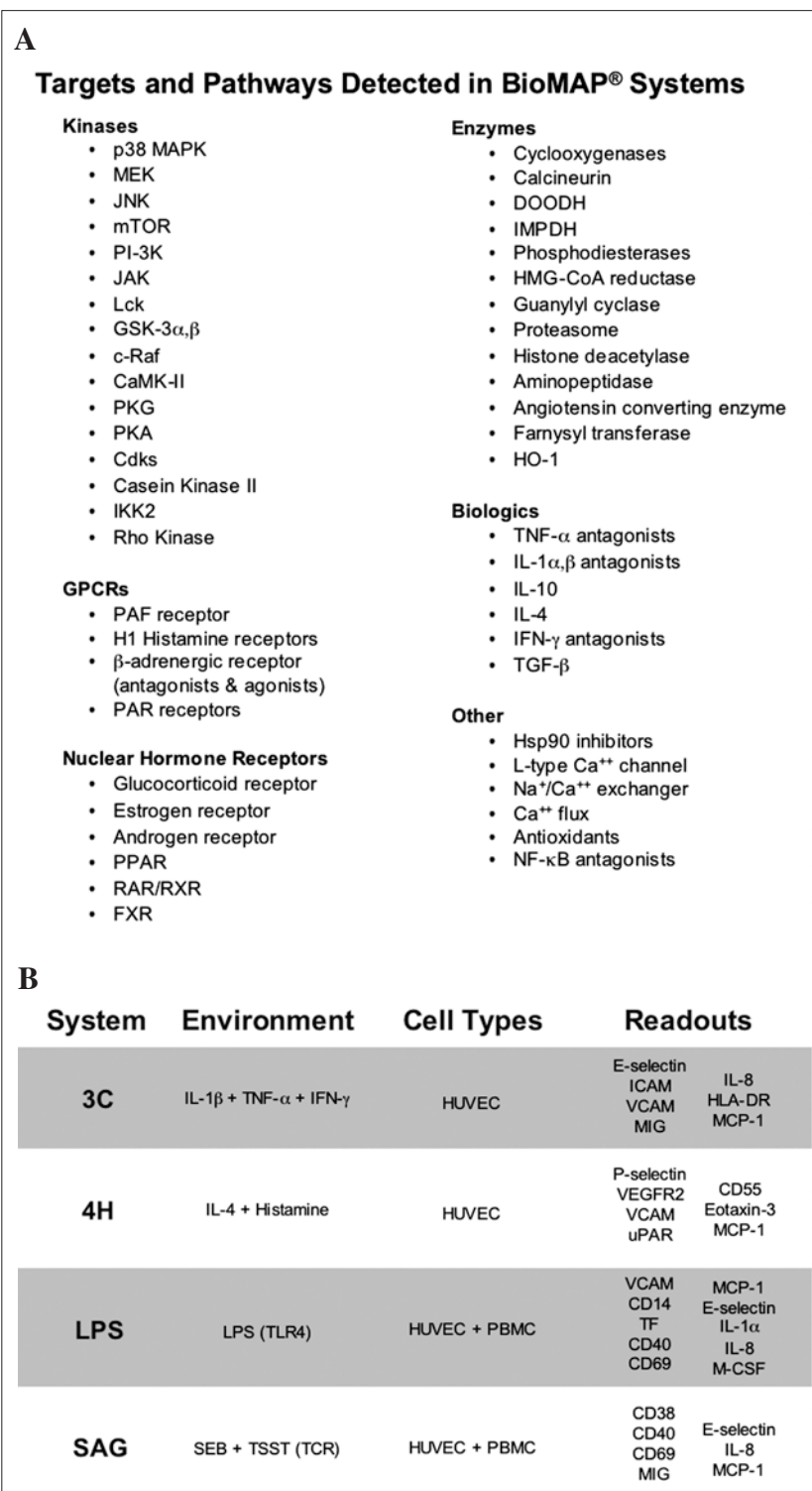


FIG. 1. Four BioMAP inflammation model systems detect and discriminate modifiers of multiple targets and pathways. **(A)** Multiple therapeutically relevant targets and pathways are detected and discriminated in BioMAP models, including a large number of kinases. **(B)** Details on the four model systems used in this article.

in Fig. 1B. Here, we focus on the application of BioMAP profiling to the characterization and SAR of kinase inhibitors.

Known pharmacologic inhibitors of several classes of kinases were evaluated in four BioMAP model systems (3C, 4H, LPS, and SAG; see Fig. 1B and *Materials and Methods* for details). Compounds (at multiple concentra-

tions) were added to cells, environmental factors were added, and after 24 h, the expression levels of proteins (readouts listed in Fig. 1B) were measured by cell-based ELISA. Figure 2A, left, shows the multisystem profiles (31 parameters) for each compound (shown for the highest, nontoxic dose) in heat map form (after log₁₀ expression ratios were calculated). Figure 2A, right, shows the

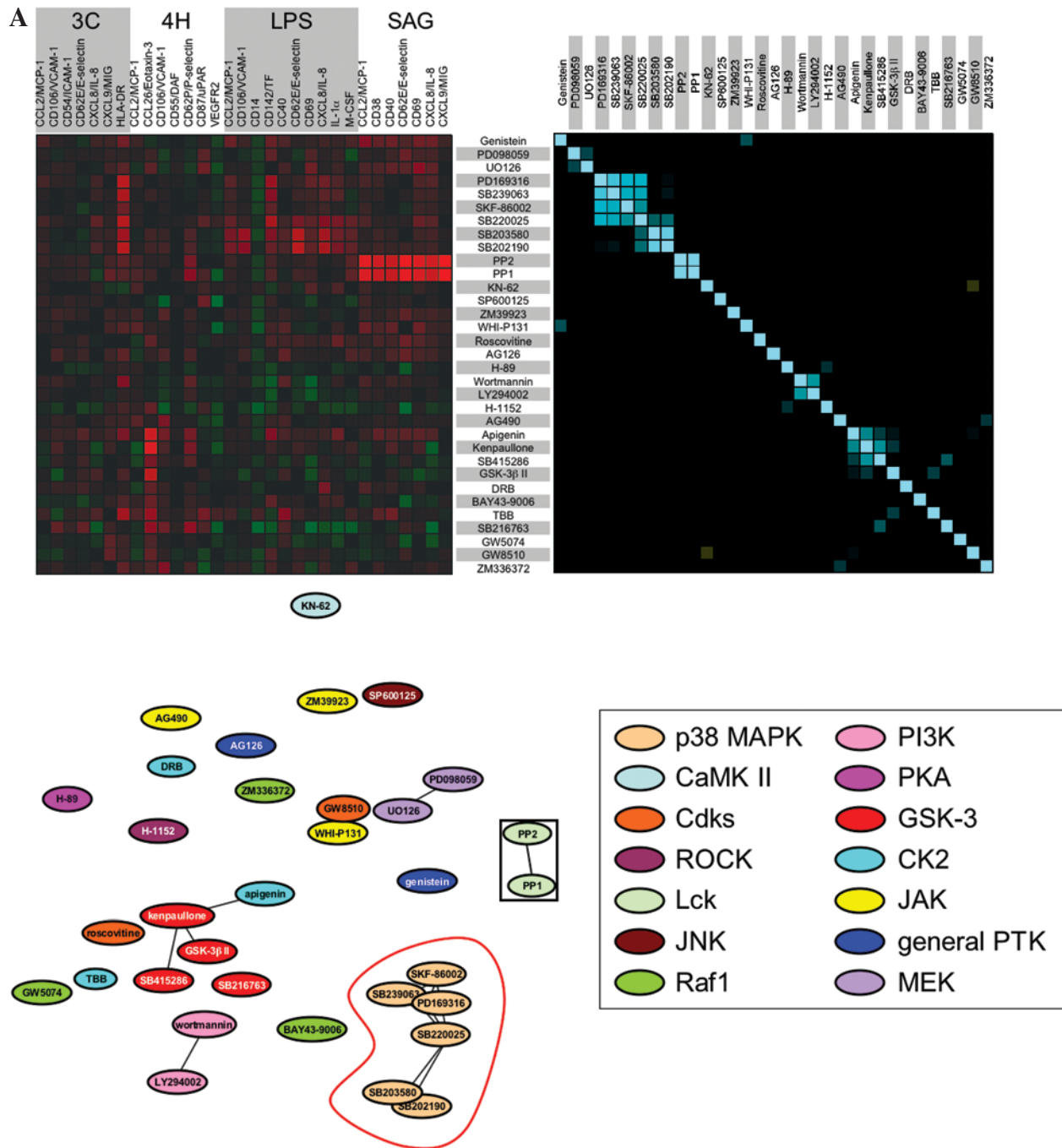


FIG. 2. Functional responses of kinase inhibitors in BioMAP inflammation systems discriminate mechanism classes. Thirty-three kinase inhibitors representing 14 distinct mechanism classes were tested in four BioMAP model systems (3C, 4H, LPS, and SAG) as described in Fig. 1B and *Materials and Methods*. (A) Heat map of mean log parameter expression ratio data from at least three experiments ($n = 3$ replicates in each experiment), showing the increase (green), decrease (red), or lack of change (black) of individual parameters for each kinase inhibitor. To the right, Pearson correlation values for pairwise comparisons of average profile data are shown: positive correlations are in blue (most intense for $r > 0.9$); black is no correlation ($r \approx 0$); and yellow indicates negative correlations. The list of compounds in (A) was ordered automatically by scaling and pivoting to move high correlations to the diagonal. (B) A Function Similarity Map is generated by subjecting the pairwise correlation data to multidimensional scaling. Significant correlations determined as described in *Materials and Methods* are shown by lines (FDR = 7%). The distance between compounds is inversely related to the similarity of the compound profiles. Compounds are color coded by reported class as shown by the legend. Compounds were tested at multiple concentrations. Data shown are at concentrations around their cellular EC_{50} (generally 10–100 times their reported biochemical IC_{50}). Doses of compounds used: genistein (10 μM), PD098059 (10 μM), UO126 (3 μM), PD169316 (1 μM), SB239063 (3 μM), SKF-86002 (3 μM), SB220025 (3 μM), SB203580 (2 μM), SB202190 (2 μM), PP2 (3 μM), PP1 (3 μM), KN-62 (3 μM), SP600125 (3 μM), ZM39923 (10 μM), WHI-P131 (10 μM), roscovitine (3 μM), AG126 (10 μM), H-89 (1 μM), wortmannin (3 μM), LY294002 (1 μM), H-1152 (1 μM), AG490 (10 μM), apigenin (3 μM), kenpaullone (1 μM), SB415286 (6 μM), GSK-3 β II (6 μM), DRB (3 μM), BAY43-9006 (0.4 μM), TBB (10 μM), SB216763 (1 μM), GW5074 (1 μM), GW8510 (0.4 μM), ZM336372 (3 μM).

pairwise Pearson correlation matrix analysis of the resulting 31 parameter profiles (averaged across three experiments). Such a correlation analysis effectively compares the “shape” of each profile, with a higher correlation for profiles that have a similar shape. In Fig. 2B, the multidimensional relationships between the various profiles are represented in two dimensions using multidimensional scaling and are visualized in a Function Similarity Map. Each oval in this plot represents a specific compound and concentration (as in Fig. 2A) with the distances between ovals inversely representative of the similarity between compounds (the closer the ovals, the more similar the compounds), with statistically significant (as described in *Materials and Methods*) correlations identified by lines connecting ovals. For some mechanistic classes, such as p38 MAPK, Lck, PI-3K, GSK-3 β , and MEK inhibitors, compounds within the same class modulate the expression of BioMAP parameters in a similar fashion (Fig. 2A) and cluster together in the Function Similarity Map (Fig. 2B). Compounds against distinct targets [e.g., KN-62 and H-89; targeting Ca²⁺/calmodulin-dependent protein kinase II (CamKII) and protein kinase A (PKA), respectively], or those known to have poor specificity for their targets or differential isoform selectivity, such as the Janus kinase (JAK) inhibitors (AG490, ZM39923, and WHI-P131), cyclin-dependent kinase (Cdk) inhibitors (roscovitine and GW8510), or general protein tyrosine kinase (PTK) inhibitors (AG126 and genistein), elicit distinctive BioMAP profiles and do not cluster together. Interestingly, significant differences were also seen among Raf1 inhibitors (BAY 43-9006, GW5074, and ZM336372) and casein kinase 2 (CK2) inhibitors (apigenin, DRB, and TBB), suggesting that these compounds also have significant off-target or secondary activities.

Discrimination of p38 MAPK inhibitors

When compared with the diverse set of bioactive kinase inhibitors in Fig. 2, inhibitors of p38 MAPK induce BioMAP profiles that are highly related to one another and form a cluster in the Function Similarity Map (indicated by the red outline in Fig. 2B), consistent with their shared selectivity for p38 MAPK. However, closer inspection of the multisystem BioMAP profiles of PD169316 and SB203580 (shown as line graphs in Fig. 3A) over a range of effective concentrations reveals consistent profile features of SB203580 that are not shared by PD169316. These features include inhibition of P-selectin expression in the 4H system, and strong inhibition of VCAM-1, E-selectin, and IL-8 in the LPS system. These activities are likely not due to differences in potency against p38 α , as the two compounds exhibit similar potencies in biochemical assays (see Fig. 4) and in the inhibition of HLA-DR expression in the 3C system.

The strong inhibition of HLA-DR appears to be an on-target effect because this activity is also observed following specific siRNA inhibition of the p38 pathway in the 3C system. As shown in Fig. 3B, an siRNA with inhibitory activity against MEK3 and MEK6, the upstream activators of p38 MAPK,^{6,7} gives the same profile as small-molecule p38 MAPK inhibitors in the 3C system, including the robust down-regulation of HLA-DR. siRNA targeting both p38 α and p38 β simultaneously was not active, possibly due to the interchangeability of these isoforms with the γ and δ isoforms or to insufficient knockdown of the proteins (data not shown).

BioMAP profiling was then used to explore the structural requirements for the activities of SB203580 identified by BioMAP analysis. Co-crystallization of SB203580 bound to p38 α ^{8,9} highlights the interaction between SB203580 chemical substituents (A, B, and C off the imidazole ring) and the ATP-binding pocket of the kinase (Fig. 4A). Whereas the fluorophenyl group of SB203580 (substituent B) has been shown to be oriented toward the “gatekeeper” residue in the ATP-binding pocket, a key determinant of small-molecule inhibitor binding specificity in kinases,⁹ substituents A and C have fewer interactions with the ATP-binding pocket and more solvent exposure. To explore structural features at positions A and C that might contribute to the activities identified for SB203580, the BioMAP profiles of several well studied p38 MAPK antagonists, including PD169316, SB202190, SB239063, and SB220025, were compared (Fig. 4). These compounds fall into two structural groups: PD169316 and SB202190, which have 4-pyridyl groups at the 5 position of the imidazole ring and contain substitution at the 4 position of the 2-phenyl ring (modifications of the C group of SB203580); and SB239063 and SB220025, which contain differently substituted pyrimidinyl groups at the 5 position of the imidazole ring, lack the 2-phenyl groups, and instead have substituted aliphatic substituents at the 1 position (modifications of both the A and C groups of SB203580) (Fig. 4A).

The Function Similarity Map in Fig. 4C shows the relationship of compound profiles at multiple doses. Compound-specific activities are revealed by differential clustering when these closely related compounds are compared with one another, rather than with the broader set of kinase inhibitors as shown in Fig. 2. In this map, the circles representing compounds are coded by color and by size according to dose. Notably, SB202190 and SB203580 show function similarity (cluster) in the central dose ranges, as do PD169316, SB220025, and SB239063 (Fig. 4C). Importantly, clustering of each compound is dose-independent over a significant concentration range (~ 10 – $20\times$), indicating that the profiles retain a characteristic shape. (Exceptions are the extreme doses of PD169316, SB202190, and SB203580, where

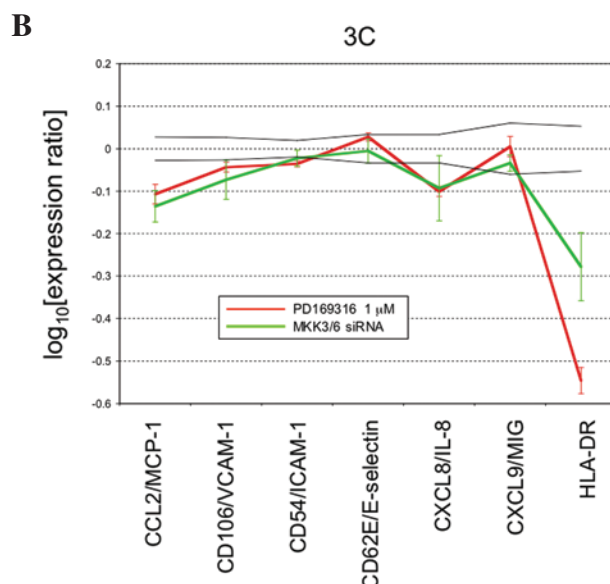
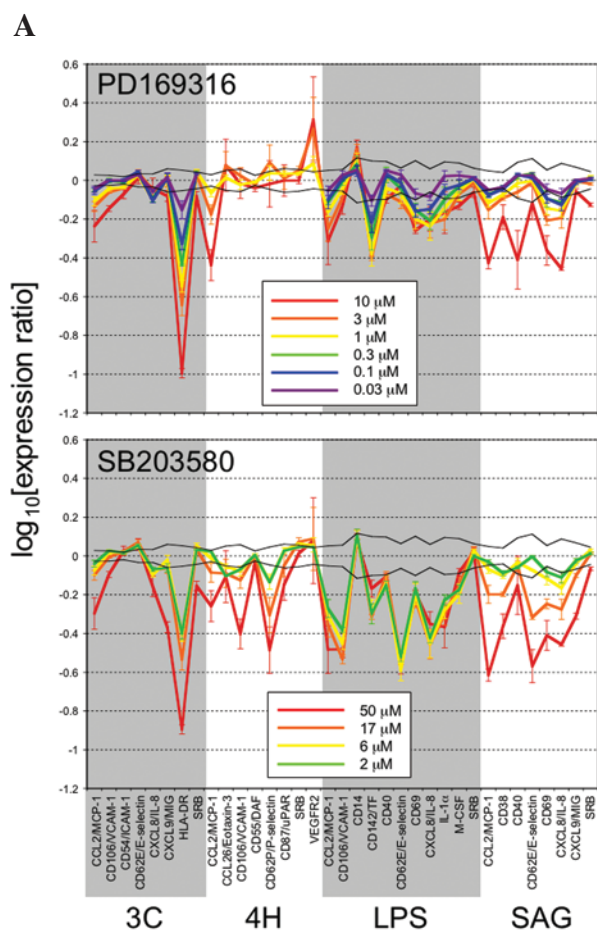


FIG. 3. p38 MAPK inhibitor profiles and on-target function validation by siRNA. (A) BioMAP profiles in four model systems for the p38 MAPK inhibitors PD169316 and SB203850 tested at multiple concentrations. Levels of protein readouts were measured by ELISA as described in *Materials and Methods* and presented as log expression ratios [$\log_{10}(\text{parameter value with drug/parameter value of control})$] relative to solvent controls. The mean and standard error are shown for each readout parameter, connected by lines for ease of visualization ($n = 3$ measurements for at least three individual experiments). (B) Comparison of the profile of PD169316 in the 3C system to siRNA knockdown of both MEK3 and MEK6 (average of three experiments). Black lines in (A) and (B) represent the 99% prediction interval of the solvent control data.

additional off-target activities or early toxic effects may contribute to profile differences.)

Inspection of the multisystem profile for each compound allows identification of the profile features that differentiate it from the other compounds. As shown in Fig. 4B, the profile plots reveal that SB202190 shares the biological activities of SB203580: inhibition of P-selectin in the 4H system and VCAM-1 and E-selectin in the LPS system, features not shared by PD169316 or SB239063 (see white arrows in Fig. 4B). The SB239063 profile is more similar to the PD169316 profile, and SB220025 has a profile that is in many regards intermediate between those of PD169316 and SB220025, except for a unique activity on CD87/uPAR in the 4H system. In this way, the comparison of BioMAP profiles of compounds tested at multiple concentrations facilitates rapid classification of compounds based on reproducible, drug-specific biological activities.

To determine how structural changes at R_1 (the substituent of SB203580 that interacts with the “gatekeeper” residue of p38) may affect the bioactivity profiles, we examined a set of analogues around SB203580 (Fig. 5) in

which the fluorophenyl group (the B substituent of SB203580 from Fig. 4A) was replaced with a series of aromatic substituents of varying steric demand (Fig. 5A). These analogues were designed to exhibit differential selectivity toward different kinases based on the established binding mode of SB203580 to its best characterized target, p38 α ,⁸ and their biochemical IC_{50} values for p38 α are shown for comparison (Fig. 5A). BioMAP analyses were carried out to assess the effects of these modifications on the biological activities (*i.e.*, profile features) and cellular potency (*i.e.*, dosing) identified for SB203580. The resulting comparison of the multisystem BioMAP profiles for each compound at four doses (5, 2, 0.6, and 0.2 μM) is shown in the Function Similarity Map in Fig. 5B. The profiles from these compounds remain clustered over a range of concentrations (except for the lowest concentrations of some analogues due to low potency, and therefore profiles that lose features retained in the higher dose range) with the exception of SK582 (orange circles), which does not cluster with the other compounds. SK582 is a very weak p38 MAPK antagonist having a biochemical IC_{50} for p38 α (10 μM) that is ~ 100 -fold lower

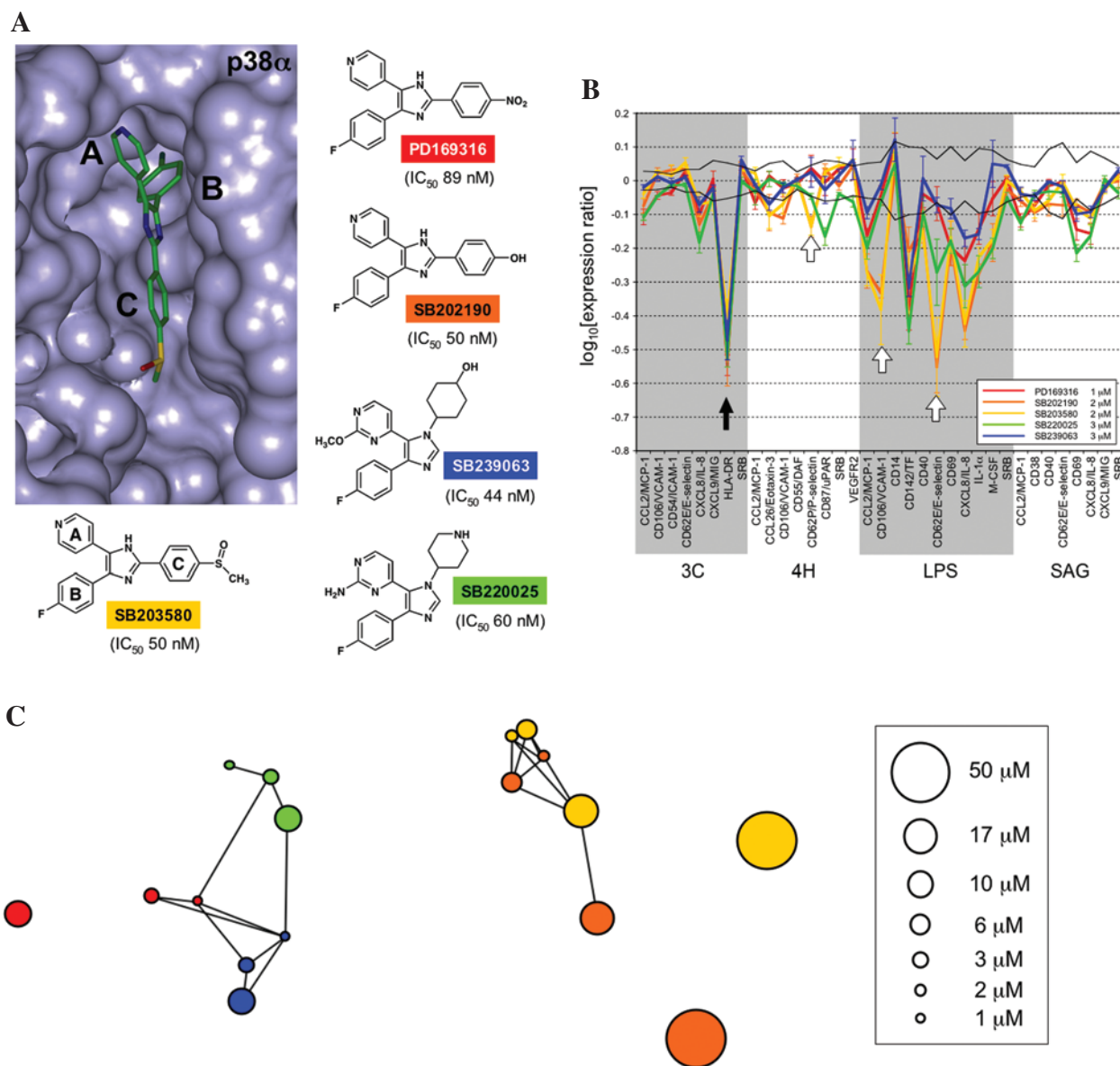
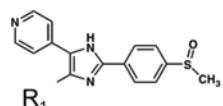


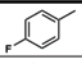
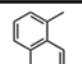
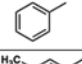
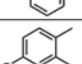
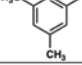
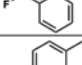
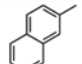
FIG. 4. Comparison of BioMAP profiles of SB203580 analogues with substituent changes at two positions. **(A)** Crystal structure of p38 α bound to the inhibitor SB203580 demonstrating the protein interaction positions of the three functional substituents (A, B, and C) off the imidazole ring. The inhibitors PD169316 and SB202190 have modifications to the C portion of SB203580, whereas SB239063 and SB220025 have modifications to the A and C positions. IC_{50} data for inhibition of biochemical p38 α activity are shown. **(B)** BioMAP profiles for one concentration of each p38 MAPK inhibitor (24-h assay). Concentrations were selected (1–3 μM) that gave a characteristic profile for each compound (clustering with other doses of the same compound) and that yielded similar inhibition of HLA-DR expression (black arrow). White arrows indicate parameters that are modulated differently by various compounds. Data are presented as log expression ratios [$\log_{10}(\text{parameter value with drug}/\text{parameter value of control})$] relative to solvent or media controls. The mean and standard error are shown for each readout parameter, connected by lines for ease of profile visualization ($n = 3$ measurements for at least three individual experiments). **(C)** A Function Similarity Map of SB203580, SB202190, PD169316, SB239063, and SB220025 at multiple concentrations. Each compound is a different color as in (A), and the area of each circle is proportional to dose. FDR = 9%.

than the other analogues. This suggests that the biological activities observed for SK582 are unlikely to be mediated by p38 MAPK inhibition, consistent with the lack of inhibition of HLA-DR expression in the 3C system by this compound. However, SK582 does retain strong

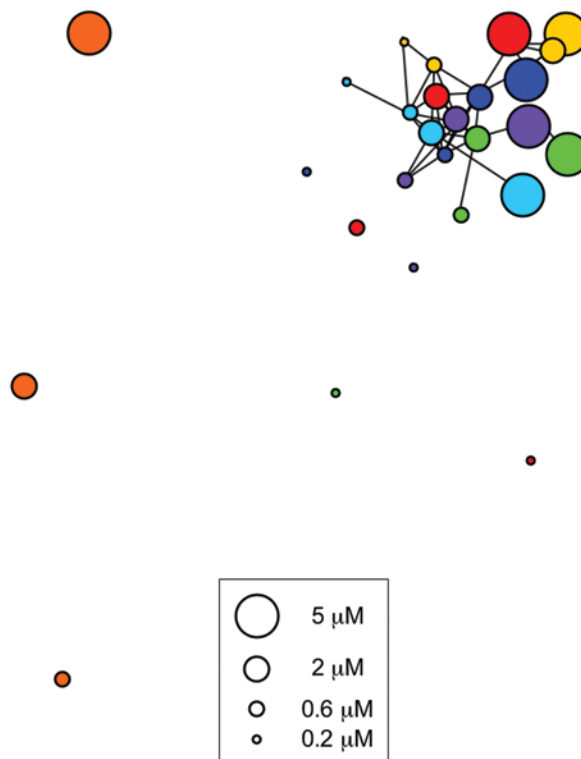
inhibitory activity on P-selectin in the 4H system, one of the features that distinguishes SB203580 from PD169316 as discussed above. This activity, isolated in the p38 MAPK-independent profile of SK582, may result from an off-target effect for SB203580, mediated by

A



Name	R ₁	Biochemical IC ₅₀ (p38α)	Name	R ₁	Biochemical IC ₅₀ (p38α)
SB203580		52 nM	SK584		140 nM
SK586		79 nM	SK587		170 nM
SK581		180 nM	SK582		10,000 nM
SK585		51 nM			

B



C

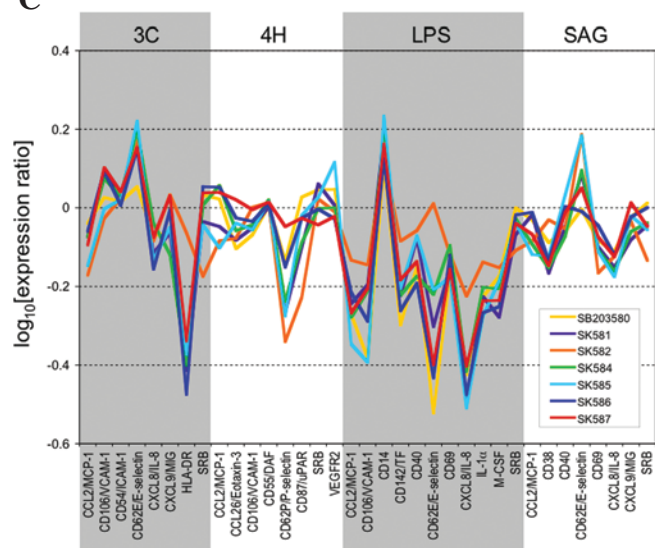


FIG. 5. SAR of SB203580 analogues with modifications of the “gatekeeper” associated fluorophenyl group. (A) Chemical modifications at the R₁ position of SB203580 and biochemical IC₅₀ data for p38α inhibition. (B) BioMAP profiles of each SB203580 analogue, tested at four concentrations, were clustered as described in *Materials and Methods*, and their relationships are represented in the Function Similarity Map. Compounds are color coded as in (A) with the circle area proportional to dose. Statistically significant correlations determined as described in *Materials and Methods* are shown by lines. FDR = 3%. (C) Profiles of each SB203580 analogue at 5 μM. The mean of *n* = 2 experiments with three wells each is shown without error bars for ease of viewing. Data are presented as log expression ratios [$\log_{10}(\text{parameter value with drug}/\text{parameter value of control})$] relative to solvent or media controls.

structural features independent of R₁ (substituent B in Fig. 4). Thus, each of the analogues in this series of R₁ variants that retain significant p38 inhibitory activity (biochemically, and as indicated by their BioMAP profiles) retains a profile similar to that of the parent compound SB203580, indicating that structural features apart from R₁ control the unique activities on E-selectin, VCAM-1, and IL-8 in the LPS system. We conclude that quantitative BioMAP profiling can be used to identify

specific structural correlates of secondary activities and to drive SAR studies of kinase inhibitors with enhanced knowledge.

Discussion

Protein kinases are an important class of therapeutic targets.¹ They comprise a large gene family, the kinome,² with some 518 members that can function as key regu-

lators in many of the important signaling pathways in disease. Kinase family members share a catalytic domain, conserved in sequence and structure, that features an ATP-binding pocket that is highly amenable to small-molecule inhibition. However, the design and selection of optimal therapeutic candidates have not been without difficulty. High affinities are required to compete with the high ATP concentrations *in vivo* and, more importantly, selectivity problems have slowed the progress of compounds in this mechanistic class and for ATP competitive inhibitors in general, because the high degree of homology between family members has led to a high frequency of secondary target effects.¹⁰

The difficulty in developing highly selective inhibitors also complicates our understanding of cell-signaling mechanisms, much of which depends on the use of specific inhibitors.¹⁰ This problem is highlighted for several classes of kinase inhibitors in the present analysis and is reflected in the poor clustering of compounds ostensibly against a common target when analyzed in BioMAP systems (*e.g.*, Cdk inhibitors, Raf1 inhibitors, CK2 inhibitors, JAK inhibitors). In many cases, this is the result of a particular compound inhibiting one or more secondary targets. For example, ZM336372 inhibits p38 MAPK kinase,¹¹ in addition to Raf1, and exhibits a unique BioMAP profile distinct from the other Raf1 inhibitors tested (GW5074 and BAY43-9006).

The selectivity problems of p38 MAPK inhibitors are well known. Off-target activities of SB203580 for Lck, Src, and cyclooxygenase-1 have been reported.^{12,13} In addition, although a number of p38 MAPK inhibitors have entered clinical trials in rheumatoid arthritis and other indications, none has yet been approved. Compounds that have not succeeded have been terminated for various reasons,¹⁴ perhaps reflecting differential off-target or secondary activities. The studies here demonstrate how chemically distinct inhibitors of p38 MAPK can be rapidly distinguished by the shared (in-target class) or unique (secondary and off-target) features of the biological responses they induce in BioMAP model systems. Secondary activities were identified for SB203580 that are shared by some, but not all, of the p38 MAPK inhibitors tested. Such additional activities may not always be liabilities and could contribute to clinical effectiveness. This appears to be the case for the kinase inhibitor, Gleevec, approved for treatment of chronic myelogenous leukemia, that inhibits c-kit and platelet-derived growth factor receptor kinases in addition to ABL.¹

BioMAP model systems can identify unexpected off-target and secondary activities and, with more knowledge of the activities of successful and failed compounds in BioMAP model systems, may prove useful for distinguishing positive from negative (undesirable) activities. We have previously described the ability of BioMAP profiling in only three systems relevant to vascular inflam-

mation to detect and distinguish the activities of compounds from a broad range of mechanism classes and therapeutic categories.³ In these biologically complex systems, pathway-pathway interactions and cell-cell communication contribute to the overall response profile, allowing pathways (and targets) that are outside the core inflammation pathways [*e.g.*, nuclear factor- κ B (NF- κ B), JAK/STAT, etc.] to be detected. This broad sensitivity may be an innate property of complex cellular systems, in which the level of each molecular or protein readout measured is an indirect reflection of pathway interactions mediated by hundreds of signaling components. The responses measured in these complex systems are surprisingly robust and reproducible, and allow the application of this approach for efficient classification of compounds according to their functional activities.

The present studies also illustrate the application of BioMAP model systems for target validation through a chemical genetics approach. As we demonstrate for p38 MAPK inhibitors, on-target activities are identified as common features of BioMAP profiles elicited by multiple, structurally distinct inhibitors, whereas off-target effects commonly include those that are not shared. However, if an inhibitor elicits a novel feature, this may result from mechanistic differences (*e.g.*, inhibitor binding to active versus inactive forms of the target) and may be a true "on target" effect. Gene knockdown with siRNA in BioMAP models can provide complementary information, although as we observed for p38 α and p38 β , results obtained from knockdown of validated targets do not always correlate with those using chemical inhibitors. siRNA can be a poor predictor of drug effects for several reasons. In addition to issues of isoform redundancy and knockdown inefficiency, which can cause siRNA experiments to fail to predict positive drug effects, knockdown can induce unexpected phenotypes by altering protein docking or signaling complex formation events that are not elicited by small-molecule inhibitors. These issues are frequently problematic for targets within signaling pathways, which often have multiple functional domains. As an alternative approach, we have previously described using BioMAP model systems for the identification and validation of new targets by gene overexpression,⁴ which allows signaling networks and feedback mechanisms to be rapidly identified.

The goal of lead optimization is the best compromise between improved activity, bioavailability, and safety of a drug. Classically, structure-activity studies in lead optimization have focused first on improvements in potency and selectivity, then subsequently on bioavailability and ADMET properties. By simultaneously addressing potency, selectivity, and favorable chemical properties (*e.g.*, solubility, permeability), BioMAP profiling is compatible with new strategies for parallel lead optimization, driven by the economic need for early attrition. As we

demonstrate here, the BioMAP profile shape can provide an informative biological measure of target specificity. As analogues of the lead compound are tested, deviations from the “parent” profile indicate likely alterations in target specificity, as well as secondary activities; as the number of different compounds against a specific target increases, so does the ability of BioMAP assays to identify truly “selective” biological effects. BioMAP analysis at multiple concentrations provides cell-based potency, therapeutic window, and toxicity information. Differences in the biological activities of compounds generated against the same target can arise from several sources: inhibition of different secondary targets, cellular uptake (differences can be cell type-specific), and mechanism of action. The BioMAP approach described here addresses all of these issues, and additionally allows for the selection of optimal compounds that may act on multiple targets, as beneficial features can often be distinguished from liabilities.

The BioMAP approach to kinase inhibitor identification and optimization has the potential to increase the speed with which compounds against kinase targets reach the clinic. BioMAP analysis can be used to quickly map biological responses to particular chemical structures, including substituents on a common scaffold. Integration of the BioMAP approach into kinase inhibitor development could be used to identify and monitor off-target and secondary activities, to define SARs, and to accelerate the design and selection of optimal therapeutic candidates. New BioMAP model systems containing additional primary cell types (*e.g.*, fibroblasts, keratinocytes, bronchial epithelial cells, mast cells, macrophages) are expanding the biology covered into additional disease areas, including fibrosis, asthma, arthritis, and psoriasis, increasing the ability of BioMAP models to be the predictive link between target validation and screening and *in vivo* studies in both animals and humans.

Acknowledgments

This work was supported in part by an SBIR grant to E.L. Berg (R43 AI048255) and an award to K.M. Shokat from the Sandler Program for Asthma Research. E.C. Butcher contributed to this work in his role as consultant to BioSeek. We thank M. Fischer, S. Privat, M. Dea, and K. Ota for excellent technical assistance.

References

1. Noble ME, Endicott JA, Johnson LN: Protein kinase inhibitors: insights into drug design from structure. *Science* 2004;303:1800–1805.

2. Manning G, Whyte DB, Martinez R, Hunter T, Sudarsanam S: The protein kinase complement of the human genome. *Science* 2002;298:1912–1934.
3. Kunkel EJ, Dea M, Ebens A, Hytopoulos E, Melrose J, Nguyen D, Ota KS, Plavec I, Wang Y, Watson SR, Butcher EC, Berg EL: An integrative biology approach for analysis of drug action in models of human vascular inflammation. *FASEB J* 2004;18:1279–1281.
4. Plavec I, Sirenko O, Privat S, Wang Y, Dajee M, Melrose J, Nakao B, Hytopoulos E, Berg EL, Butcher EC: Method for analyzing signaling networks in complex cellular systems. *Proc Natl Acad Sci USA* 2004;101:1223–1228.
5. Bishop AC: *Chemical Genetic Approaches To Highly Selective Protein Kinase Inhibitors*. Princeton University, Princeton, NJ, 2000.
6. Jiang Y, Chen C, Li Z, Guo W, Gegner JA, Lin S, Han J: Characterization of the structure and function of a new mitogen-activated protein kinase (p38beta). *J Biol Chem* 1996;271:17920–17926.
7. Raingeaud J, Whitmarsh AJ, Barrett T, Derijard B, Davis RJ: MKK3- and MKK6-regulated gene expression is mediated by the p38 mitogen-activated protein kinase signal transduction pathway. *Mol Cell Biol* 1996;16:1247–1255.
8. Tong L, Pav S, White DM, Rogers S, Crane KM, Cywin CL, Brown ML, Pargellis CA: A highly specific inhibitor of human p38 MAP kinase binds in the ATP pocket. *Nat Struct Biol* 1997;4:311–316.
9. Wilson KP, McCaffrey PG, Hsiao K, Pazhanisamy S, Galullo V, Bemis GW, Fitzgibbon MJ, Caron PR, Murcko MA, Su MS: The structural basis for the specificity of pyridinylimidazole inhibitors of p38 MAP kinase. *Chem Biol* 1997;4:423–431.
10. Bain J, McLauchlan H, Elliott M, and Cohen P: The specificities of protein kinase inhibitors: an update. *Biochem J* 2003;371:199–204.
11. Hall-Jackson CA, Evers PA, Cohen P, Goedert M, Boyle FT, Hewitt N, Plant H, Hedge P: Paradoxical activation of Raf by a novel Raf inhibitor. *Chem Biol* 1999;6:559–568.
12. Wadsworth SA, Cavender DE, Beers SA, Lalan P, Schaffer PH, Malloy EA, Wu W, Fahmy B, Olini GC, Davis JE, Pellegrino-Gensey JL, Wachter MP, Siekierka JJ: RWJ 67657, a potent, orally active inhibitor of p38 mitogen-activated protein kinase. *J Pharmacol Exp Ther* 1999;291:680–687.
13. Borsch-Haubold AG, Pasquet S, Watson SP: Direct inhibition of cyclooxygenase-1 and -2 by the kinase inhibitors SB 203580 and PD 98059. SB 203580 also inhibits thromboxane synthase. *J Biol Chem* 1998;273:28766–28772.
14. Palladino MA, Bahjat FR, Theodorakis EA, and Moldawer LL: Anti-TNF α therapies: The next generation. *Nat Rev Drug Discov* 2003;2:736–746.

Address reprint requests to:

Ellen L. Berg, Ph.D.
Chief Scientific Officer
Bioseek, Inc.
863-C Mitten Rd.
Burlingame, CA 94010

E-mail: eberg@bioseekinc.com